# Valence-bond analysis of extended Hubbard models: Charge-transfer excitations of molecular conductors

S. Mazumdar and Z. G. Soos
*Department of Chemistry, Princeton University, Princeton, New Jersey 08544*
(Received 19 May 1980)

The low-energy charge transfer (CT) excitation characteristic of both $\pi$-molecular conductors and complex-ion-radical salts is interpreted as a nearest-neighbor Coulomb interaction $V$ that is comparable to the bandwidth, $4|t|$. Partly filled segregated regular stacks in organic conductors are represented by extended Hubbard models, whose exact CT energies and intensities are obtained by diagrammatic valence-bond (VB) methods for four electrons on finite rings and chains, together with an approximate treatment of $V$ in partly filled infinite stacks for infinite on-site correlations $U$. Finite $V \sim 4|t|$ yields an intense low-lying CT band, containing $V$ and $U-2V$ excitations, that depends weakly on the band filling. Finite $V$ also splits the usual CT absorption around $U$ for half filled bands into strong absorptions around $U-V$, weak ones around $U$, and much weaker bands around $U+V$ and $U+2V$. The CT spectra of mixed-valence tetrathiofulvalene (TTF) salts are modeled with $V \sim 0.4$ eV, $U \sim 1.4$ eV, and $|t| \sim 0.10$–$0.13$ eV. Similar CT transitions in complex tetracyanoquinodimethane (TCNQ) salts are consistent with the insensitivity of the $V$ peak's position to the filling or the structure. Restricting the basis to one valence state per site produces several general consequences for dipole-allowed optical transitions.

## I. INTRODUCTION

There is great current interest[1,2] in the magnetic, transport, and structural properties of $\pi$-molecular organic solids based on acceptors like tetracyanoquinodimethane (TCNQ) or chloranil and donors like tetrathiofulvalene (TTF) or *NNN'N'* -tetramethyl-*p*-phenylenediamine (TMPD). While quantitative results remain elusive, a classification[3] of electronic properties has provided a useful qualitative framework. These organic solids crystallize in face-to-face arrays of planar $A$, $A^-$, $D$, or $D^+$ molecules, with significant $\pi$ overlap indicated along the stack by close contacts of 3–3.5 Å and typical van der Waals separations between stacks. The first classification[4] is consequently into *segregated* stacks containing all $A$'s or all $D$'s and *mixed* $\cdots DADA \cdots$ stacks. The second classification[5] is into *regular* stacks containing a single charge-transfer (CT) interaction $|t|$ and *alternating* (dimerized, trimerized, tetramerized) stacks with several $|t|$'s and triplet spin excitons. The third classification involves the stoichiometry[6] or the degree[3] of CT in the ground state. *Simple,* or half filled, stacks contain $A^-$ or $D^+$ radicals and exhibit a single CT absorption; *complex,* or mixed-valence, salts contain $A^{-\gamma}$ or $D^{+\gamma}$ stacks with $\gamma < 1$ and show additional, low-energy CT excitations[7] that can be associated with electron transfer from ionic to neutral species. These three criteria produce eight classes, most of which are realized experimentally.[3] Thus all organic conductors are segregated complex regular systems. Further distinctions within a given class must be considered for semiquantitative applications.

The underlying physical picture[3] is one of weakly overlapping molecular solids with a modest bandwidth $4|t| \sim 0.5$ eV along the stack and on-site correlations $U > 4|t|$ against doubly occupied $A^{-2}$ sites or doubly ionized $D^{+2}$ sites. Correlations in narrow-band solids suggest a valence-bond (VB) description for extended versions of Hubbard models[8] in the difficult intermediate regime[3,9] $U \sim 4|t|$ where band-theoretical results are suspect. Although restricted to finite systems, diagrammatic VB methods describe correlations in mixed stacks,[10] in segregated stacks,[11] and in magnetic insulators.[12] Such numerical methods give both energies and wave functions, thus yielding[13] the position and intensity of CT transitions.

We focus here on the CT spectra of segregated complex stacks. These $\cdots A^{-\gamma}A^{-\gamma}A^{-\gamma}\cdots$ or $\cdots D^{+\gamma}D^{+\gamma}D^{+\gamma}\cdots$ systems have a single CT integral $|t|$, a nonintegral ionicity $\gamma < 1$, and additional low-energy CT transitions. Torrance *et al.*[14] and Tanaka *et al.*[15] have carefully examined the optical properties of a number of TCNQ and TTF salts, in several instances augmenting previous powder data with single-crystal reflectivity data. Their results are summarized in Table I, together with related optical data on complex salts.[16] Molecular ($\pi \rightarrow \pi^*$) transitions of TCNQ or $TCNQ^-$ are polarized in plane and begin around 1.5 eV, the in-plane $\pi \rightarrow \pi^*$ transitions of TTF or $TTF^+$ start around 2.2 eV.[14] The polariza-

TABLE I. Low-energy optical properties of representative TTF and TCNQ crystals.

| System | Filling $\gamma$ | CT Absorptions $A$ (eV) | $B$ (eV) | Ref. | Comment Structure/Conductivity |
|---|---|---|---|---|---|
| TTF-$Cl_{1.0}$ | 1.0 | · · · | 1.5 | 14 | Dimers; insulator |
| TTF-$Cl_{0.80}$ | 0.80 | 0.59 | 1.5 | 14 | Incommensurate regular $TTF^{+\gamma}$ and $X^-$ arrays; conductors with complicated temperature dependences |
| TTF-$Br_{0.79}$ | 0.79 | 0.59 | 1.5 | 14 | |
| TTF-$I_{0.71}$ | 0.71 | 0.52 | 1.5 | 14 | |
| Rb-TCNQ(II) | 1.0 | · · · | 1.05 | 15 | Regular stack; phase II; insulator |
| $Cs_2(TCNQ)_3$ | 0.67 | 0.45 | 1.45 | 16 | Trimerized stacks; |
| | | 0.74 | 1.36 | 15 | Semiconductor |
| $(Mor)_2(TCNQ)_3$[a] | 0.67 | 0.68 | 1.49 | 15 | Trimerized; semiconductor |
| $(TEA)(TCNQ)_2$[b] | 0.50 | 0.4 | 1.4 | 16 | Tetramerized; small gap semiconductor |
| $Q(TCNQ)_2$ | 0.50 | 0.68 | 1.5 | 15 | Regular, cationic disorder; activated mobility; conductors at 300 K. |
| NMP-TCNQ[c] | ~0.9 | 0.5 | 1.4 | 16 | |
| TTF-TCNQ | 0.59 | 0.35 | 1.4 | 16 | Regular; two-stack conductor, power law $T > 60$ K |

[a]Mor = morpholinium. [b]TEA = triethylammonium. [c]NMP = *N*-methylphenazinium.

tion of the CT transitions $A$ and $B$ in Table I along the stack thus supports their usual[3,7,14] interpretation as CT processes. The $B$ transition is the usual Mulliken CT band for dimers[17] and also occurs in simple ($\gamma = 1$) salts like K-TCNQ or TTF-Cl. As usual with $\pi$-radical solids, other mechanisms have been suggested and Tanaka *et al.*[15] associate the $B$ transition with molecular excitations arising from the fact that the molecular planes are not perpendicular to the stack.

Diagrammatic VB methods[10,11,13] permit a more quantitative analysis of the $A$ transition of complex salts in Table I. The extensive configuration interaction (CI) among $A$, $A^-\alpha$, $A^-\beta$, and $A^{-2}$ sites in $TCNQ^{-\gamma}$ stacks and among $D$, $D^+\alpha$, $D^+\beta$, and $D^{+2}$ sites in $TTF^{+\gamma}$ stacks can be treated exactly, albeit in rather small systems. We relate the $A$ transition in Table I to a Coulomb interaction $V$ between electrons on adjacent sites. A significant $V$ of the order of $4|t|$ in turn affects the higher-energy $B$ transition. The analysis of CT excitations, and especially of the $A$ transition, in segregated complex regular stacks with both on-site ($U$) and nearest-neighbor ($V$) correlations is developed in this paper.

We note that Table I suggests a common electronic origin like $V$ for the $A$ peak. The point is that similar spectra are seen in complex salts whose structural and transport properties are quite different. The trimerized $Cs_2(TCNQ)_3$ and tetramerized TEA $(TCNQ)_2$ salts are semiconductors and show triplet spin excitons. The acridinium (Ad) and quinolinium (Q) salts have disordered cations, a modest region of high conductivity around 300 K, and power-law magnetic properties at low temperature. The organic conductors TTF-TCNQ, TSeF-TCNQ, and TTF-$X_\gamma$ are again different. The insensitivity of the $A$ transition of complex salts to the ionicity $0.5 \leqslant \gamma < 1.0$ or to the structure is strong qualitative evidence for a common origin involving neither $\gamma$ nor the structure.

The electronic states of extended Hubbard models for densities $0.5 \leqslant \gamma < 1.0$ are developed in Sec. II in a manner quite analogous to Hubbard's original treatment[8] of on-site correlations. Their optical properties are summarized in Sec. III and are illustrated by VB computations on finite chains and rings. The resulting picture of complex ion-radical salts is discussed in Sec. IV. The emphasis has deliberately been restricted to explicit solutions of extended Hubbard models, thereby omitting extensions to various electron-phonon interactions, to long-range Coulomb interactions (screening), or to higher-energy molecular excitations. We focus instead on the role of correlations for optical properties of partly filled regular stacks.

## II. PARTLY FILLED EXTENDED HUBBARD MODEL

Metals have partly filled valence bands, while insulators and semiconductors have a finite-energy gap, $2\Delta E_c$, between a filled valence band and an empty conduction band. Mott argued[18] that correlations decisively alter this elementary picture in the limit of narrow bands. At large separations $R$, a hypothetical regular array of H atoms dissociates into neutral atoms, with $2\Delta E_c \simeq I - A = 13$ eV required to produce a separated electron-hole pair. Regular arrays with one valence electron are metallic at small $R$, as illustrated by alkali metals. The crossover from a band, or MO, to a localized, or VB, description remains mathematically intractable for realistic long-range Coulomb interactions. Hubbard models[8] discard all correlations except the on-site interaction

$U > 0$ for two electrons at the same site. Even then, exact results are restricted to one-dimensional arrays.

In the simplest case of one valence state per site, the Hubbard model for a regular segregated stack is

$$\mathcal{H}_{\rm Hu} = -|t| \sum_{p\sigma} (a^{\dagger}_{p\sigma} a_{p+1\sigma} + a^{\dagger}_{p+1\sigma} a_{p\sigma}) + U \sum_{p} a^{\dagger}_{p\alpha} a^{\dagger}_{p\beta} a_{p\beta} a_{p\alpha} \quad . \tag{1}$$

The fermion operators $a^{\dagger}_{p\sigma}$ ($a_{p\sigma}$) create (annihilate) electrons in the valence state of the $p$th site. All intrasite electronic correlations can be included formally[19] when the parameters $|t|$ and $U$ are defined phenomenologically.[3] The $U = 0$, or band, limit of Eq. (1) is sketched in Fig. 1 and consists of $2N$ tight-binding states.

$$\epsilon_{k\sigma} = -2|t| \cos kc \tag{2}$$

for $-\pi < kc \leq \pi$ in the first Brillouin zone and a spacing $c$ along the regular array. The $U \rightarrow \infty$, or atomic, limit[20] of Eq. (1) leads to subbands involving various numbers of doubly occupied sites. The lowest subband in the atomic limit is, as shown in Fig. 1, again given by Eq. (2), with only $N$ states for *spinless* fermions. Neither of these exact limits is satisfactory for $\pi$-radical solids: the band ($U = 0$) limit incorrectly predicts that half filled regular systems are metallic, while the atomic ($U \rightarrow \infty$) limit incorrectly predicts Currie-law static susceptibilities. They nevertheless provide starting places for discussing the different regime $U \sim 4|t|$ where correlations are comparable to the bandwidth. The exact ground-state energy[21] and excitations[22] of Eq. (1) are known for arbitrary $U/|t|$ and for arbitrary filling.[23] There is a single CT absorption around $U$ for any $\gamma$.

The low-energy absorption of the complex salts in Table I thus requires extending Eq. (1) to include additional Coulomb interactions or lattice vibrations. We develop the former alternative here and introduce Coulomb interactions $V_n$ among electrons $n$ sites apart, as in Pariser-Parr-Pople (PPP) model[24] for polyenes. Since estimates of $V_n$ for $n \geq 2$ in organic solids indicate that at most $V_1$ is comparable to $4|t|$, we limit discussion to $V_1 = V$ and augment Eq. (1) by

$$\mathcal{H}_1 = V \sum_{p} n_p n_{p+1} \quad , \tag{3}$$

where $n_p = a^{\dagger}_{p\alpha} a_{p\alpha} + a^{\dagger}_{p\beta} a_{p\beta}$ is the number operator. Previous treatments[25] of the extended Hubbard model dealt primarily with the $|t| = 0$ limit and/or $\gamma = 1$ or $\frac{1}{2}$. Hubbard[26] has discussed the Wigner lattices arising from the $t = 0$, $U = \infty$ limit when additional $V_n$ are retained. This limit is hardly appropriate for $\pi$-radical solids, whose interesting magnetic and transparent properties reflect $\pi$ overlap, and thus finite $|t|$, along a one-dimensional array.

For simplicity, we consider the reduced Hamiltonian

$$\mathcal{H}_{\rm red} = V \sum_{p} n_p n_{p+1} + t \sum_{p} (c^{\dagger}_{p} c_{p+1} + c^{\dagger}_{p+1} c_{p}) \tag{4}$$

involving the $U = \infty$ limit of Eq. (1). Finite $U$ calculations are deferred to Sec. III. The operators $c^{\dagger}_{p}$, $c_p$ in Eq. (4) describe spinless fermions and $n_p$ is now restricted to 0 or 1. For $N$ sites and $N_e = \gamma N$ electrons, we seek solutions to Eq. (4) with a given number of fermions,

$$\gamma = N^{-1} \sum_{p} n_p \quad . \tag{5}$$

In the special case $\gamma = 0.5$, des Cloizeaux and Gaudin[27] solved Eq. (4) exactly in terms of an equivalent spin problem. The excitation spectrum has no gap for $V \leq 2|t|$ and a gap of order $V$ for $V >> 2|t|$. There are no exact results, even for $\gamma = 0.5$, for finite $U$.

We anticipate a gapless excitation spectrum for $\mathcal{H}_{\rm red}$ for intermediate ionicity $0.5 < \gamma < 1.0$. The following approximate solution of $\mathcal{H}_{\rm red}$ is exact at both $t = 0$ and $V = 0$ and parallels the original[8] treatment of on-site correlations $U$. The two-time retarded (+) and advanced (−) Green's functions $\langle\langle A(t);B(t')\rangle\rangle^{(\pm)}$ are defined[28] as

$$\langle\langle A(t);B(t')\rangle\rangle^{(\pm)} = \mp i\Theta(\pm(t-t'))\langle [A(t),B(t')]_{\eta}\rangle \quad . \tag{6}$$

Here $[A,B]_{\eta}$ is the commutator ($\eta = -$) or anticommutator ($\eta = +$), whichever is more convenient, of two operators $A$ and $B$; $\langle\ \rangle$ denotes the thermodynamic average; and the step function $\Theta(x)$ satisfies

$$\Theta(x) = \begin{cases} 1, & x > 0 \\ 0, & x < 0 \end{cases} \quad . \tag{7}$$

This simple Green's function is related to more complicated Green's functions through its equation of motion

$$E\langle\langle A;B\rangle\rangle_E = (2\pi)^{-1}\langle [A,B]_{\eta}\rangle + \langle\langle [A,\mathcal{H}];B\rangle\rangle_E \quad , \tag{8}$$

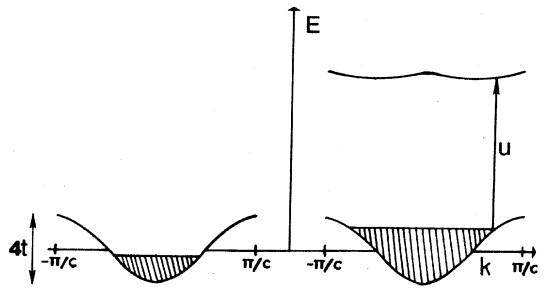


FIG. 1. Schematic representation of a normal, partly filled metallic band the resulting Hubbard subbands for on-site correlations $U$ large compared to the bandwidth $4|t|$. The usual CT transition is around $U$.

where $\langle\langle A;B\rangle\rangle_E$, the Fourier transform of the retarded and advanced Green's functions, is defined over the complete energy axis. The Green's function for sites $p$ and $q$

$$G_{pq}(E)=\langle\langle c_p(t);c_q(t')\rangle\rangle_E \tag{9}$$

is related to the density of states $\rho(E)$ per site through

$$\rho(E)=\frac{i}{N}\lim_{\epsilon\to 0+}\sum_p[G_{pp}(E+i\epsilon)-G_{pp}(E-i\epsilon)] \ . \tag{10}$$

We now find $G_{pq}(E)$ and $\rho(E)$ for $\mathcal{H}_{\rm red}$ by modifying the treatment of on-site correlations.

### A. Zero bandwidth

The $|t|=0$ limit of Eq. (4) yields $\mathcal{H}_1$ and is exactly soluble. Its development here draws attention to specific correlations that persist for the more interesting case of $|t|>0$. For $t=0$, the number operators $n_p$ are conserved, with $[\mathcal{H}_1,n_p]=0$. We also have

$$[c_p,\mathcal{H}_1]=V(n_{p+1}+n_{p-1})c_p \ . \tag{11}$$

The equation of motion (8) now yields

$$EG_{pq}^{(0)}(E)=(2\pi)^{-1}\delta_{pq}+V[\Gamma_{pq}(E)+\Pi_{pq}(E)] \ , \tag{12}$$

where we have defined

$$\begin{aligned}\Gamma_{pq}(E)&=\langle\langle n_{p+1}c_p;c_q^\dagger\rangle\rangle_E \ ,\\ \Pi_{pq}(E)&=\langle\langle n_{p-1}c_p;c_q^\dagger\rangle\rangle_E \ .\end{aligned} \tag{13}$$

We note that $\Gamma_{pq}=\Pi_{pq}$ by symmetry. Again using the equation of motion leads to

$$\begin{aligned}E\Gamma_{pq}(E)=&(2\pi)^{-1}\delta_{pq}\langle n_{p+1}\rangle-(2\pi)^{-1}\delta_{p+1,q}\langle c_{p+1}^\dagger c_p\rangle\\&+V\Gamma_{pq}(E)+V\langle\langle n_{p+1}n_{p-1}c_p;c_j^\dagger\rangle\rangle_E \ .\end{aligned} \tag{14}$$

The equation for $\Pi_{pq}$ is identical to Eq. (14), except for replacing $p+1$ by $p-1$ everywhere. The term $\langle c_{p+1}^\dagger c_p\rangle$ vanishes for $|t|=0$.

The propagator $G_{pq}^{(0)}(E)$ describes the motion of a particle being added to the system. When only on-site ($U$) correlations are considered, the injected electron goes either to an empty or a singly occupied site; the former does not change the total energy, while the latter increases it by $U$. The result of adding an electron is then virtually identical with moving an electron already in the system. This is no longer the case for nearest-neighbor ($V$) correlations. Now an electron transfer can at most raise the energy by $V$, while adding an electron between two singly occupied sites increases the energy by $2V$. The point is that an electron transferred to site $p$ must originate at either site $p+1$ or $p-1$. Conversely, either $p+1$ or $p-1$ must be empty for an electron to leave site $p$, when $U=\infty$. The number operators $n_{p+1}$ and $n_{p-1}$ are thus strongly correlated and either one or the other *must* vanish in $(n_{p+1}+n_{p-1})c_p$. We consequently have the exact, though *ad hoc*, result

$$\langle\langle n_{p+1}n_{p-1}c_p;c_q^\dagger\rangle\rangle_E=0 \ , \tag{15}$$

which further simplifies Eq. (14). In addition the $\langle n_{p+1}\rangle=\langle n_{p-1}\rangle$ expectation value is $\frac{1}{2}\gamma$ for sites adjacent to $p$, whereas the usual result $\langle n_r\rangle=\gamma$ holds for other expectation values. This simplifies Eq. (14) to

$$E\Gamma_{pq}(E)=(4\pi)^{-1}\gamma+V\Gamma_{pq}(E) \ . \tag{16}$$

$\Pi_{pq}(E)$ satisfies an identical equation. Substituting Eq. (16) into Eq. (12) yields

$$G_{pq}^{(0)}(E)=\frac{\delta_{pq}}{2\pi}\left[\frac{1-\gamma}{E}+\frac{\gamma}{E-V}\right] \ , \tag{17}$$

where the superscript is a reminder of zero-bandwidth limit. The resulting density of states is

$$\rho^{(0)}(E)=(1-\gamma)\delta(E)+\gamma\delta(E-V) \ . \tag{18}$$

The $t\to 0$ limit has states at $E=0$ and at $E=V$, as expected from $\mathcal{H}_1$ for electrons at sites next to empty and occupied sites, respectively.

The density of states at $E=0$ is $1-\gamma$, while the density at $E=V$ is $\gamma$. The Fermi energy is initially fixed at $\mu=0$ as the lower level is filled up and every other site is occupied. The lower level is filled for $\gamma=1-\gamma$, or $\gamma=0.5$, when the chemical potential jumps to $\mu=V$. In contrast to the lower subband of the Hubbard model (1), the ground state of $\mathcal{H}_1$ is doubly degenerate at $\gamma=0.5$, since there are two ways of occupying every other site. This effect persists for finite $|t|$, where $\mathcal{H}_1$ again splits the lower subband of Eq. (1) without breaking the symmetry.

### B. Finite bandwidth

The relevant commutators of $n_p$ or $c_p$ with the reduced Hamiltonian (4) generalize Eq. (12) to

$$EG_{pq}(E)=EG_{pq}^{(0)}(E)+t[G_{p+1,q}(E)+G_{p-1,q}(E)] \ . \tag{19}$$

$\Gamma_{pq}(E)$ and $\Pi_{pq}(E)$ are now coupled to higher-order Green's functions. In addition to the terms in Eq. (14), $E\Gamma_{pq}(E)$ now contains

$$\begin{aligned}t[&\langle\langle n_{p+1}c_{p+1};c_q^\dagger\rangle\rangle_E+\langle\langle n_{p+1}c_{p-1};c_q^\dagger\rangle\rangle_E\\&+\langle\langle(c_{p+1}^\dagger c_{p+2}-c_{p+2}^\dagger c_{p+1}+c_{p+1}^\dagger c_p-c_p^\dagger c_{p+1})c_p;c_q^\dagger\rangle\rangle_E] \ .\end{aligned} \tag{20}$$

A similar contribution is found for $E\Pi_{pq}(E)$, with $p\mp m$ replacing $p\pm m$. The strong restriction on $n_{p+1}+n_{p-1}$ discussed above is a consequence of the

$U=\infty$ limit and persists for finite bandwidths. Thus Eq. (15) is again found. It also follows exactly from the definition (9) that

$$\langle\langle n_{p+1}c_{p+1};c_q^\dagger\rangle\rangle_E=\langle\langle c_{p+1}^\dagger c_p c_p;c_q^\dagger\rangle\rangle_E=0 \quad . \tag{21}$$

This simplifies somewhat the contributions (20) for finite $|t|$.

No approximations have been made yet. The remaining higher-order Green's function in Eq. (20) produce a hierarchy that precludes exact results. We decouple by following Hubbard's approximations[8] for on-site correlations. Our approximations are

$$\langle\langle n_{p+1}c_{p-1};c_q^\dagger\rangle\rangle_E=\langle n_{p+1}\rangle G_{p-1,q}(E) \quad , \tag{22}$$

$$\langle\langle c_{p+1}^\dagger c_{p+2}c_p;c_q^\dagger\rangle\rangle_E=\langle c_{p+1}^\dagger c_{p+2}\rangle G_{pq}(E) \quad , \tag{23}$$

$$\langle\langle c_{p+2}^\dagger c_{p+1}c_p;c_q^\dagger\rangle\rangle_E=\langle c_{p+2}^\dagger c_{p+1}\rangle G_{pq}(E) \quad . \tag{24}$$

In Eq. (22), we separate operators for uncorrelated sites, while in Eqs. (23) and (24) we decouple operators for correlated sites. These are the simplest approximations[8] that still yield the exact $t=0$ results and can also be expected to give reasonable results for large $V$.

Having decoupled in Eqs. (22), (23), and (24), we note that $\langle n_{p+1}\rangle=\gamma$ and that $\langle c_{p+1}^\dagger c_{p+2}\rangle=\langle c_{p+2}^\dagger c_{p+1}\rangle$ by symmetry. The equations of motion (16) and (20) for $\Gamma_{pq}(E)$ then reduce to

$$\begin{aligned}E\Gamma_{pq}(E)=&(4\pi)^{-1}\gamma\delta_{pq}-(2\pi)^{-1}\delta_{p+1,q}\langle c_{p+1}^\dagger c_p\rangle\\&+V\Gamma_{pq}(E)+\gamma tG_{p-1,q}(E)\\&+t\langle\langle n_p c_{p+1};c_q^\dagger\rangle\rangle \quad .\end{aligned} \tag{25}$$

No replacement has been made for the last term in Eq. (20), which corresponds to $\Pi_{p+1,q}(E)$. Using the approximations above, we obtain a similar equation of motion for $\Pi_{p+1,q}(E)$. Combining this with Eq. (25) gives

$$\begin{aligned}\left[E-V-\frac{t^2}{E-V}\right]\Gamma_{pq}(E)=&(4\pi)^{-1}\gamma\delta_{pq}-(2\pi)^{-1}\Phi\delta_{p+1,q}+\gamma tG_{p-1,q}(E)\\&+\frac{t}{E-V}[(4\pi)^{-1}\gamma\delta_{p+1,q}-(2\pi)^{-1}\Phi\delta_{pq}+\gamma tG_{p+2,q}(E)] \quad ,\end{aligned} \tag{26}$$

with $\Phi=\langle c_{p+1}^\dagger c_p\rangle$. A similar development yields for $\Pi_{pq}(E)$. Substituting into Eq. (19) and Fourier transforming the resulting equation leads to

$$2\pi NG(k,E)=\frac{E-V(1-\gamma)+2V\Phi_k\cos kc-\frac{t}{E-V}(t+2V\Phi_k)}{(E-V)(E-2\cos kc)-2V\gamma t\cos kc-\frac{t^2}{E-V}(E-2t\cos kc-2V\gamma\cos 2kc)} \quad . \tag{27}$$

We have used the definitions

$$\begin{aligned}G_{pq}(E)&=N^{-1}\sum_k G(k,E)\exp ik(p-q)c \quad ,\\ \Phi&=N^{-1}\sum_k\Phi_k\exp ikc \quad ,\end{aligned} \tag{28}$$

with $-\pi<kc\leq\pi$ in the first Brillouin zone.

The result [Eq. (27)] for $G(k,E)$ is exact for both $t=0$, when $\Phi_k$ also vanishes, and for $V=0$, when $G(k,E)$ reduces to $(2\pi N\epsilon_k)^{-1}$ with $\epsilon_k$ given in Eq. (2). For strong correlations (large $V$), the last term in the demoninator of Eq. (27) can be neglected. The poles of $G(k,E)$ then give the energies

$$\begin{aligned}2E_k^\pm=&(V+2t\cos kc)\\&\pm[(V+2t\cos kc)^2-8(1-\gamma)Vt\cos kc]^{1/2} \quad .\end{aligned} \tag{29}$$

We obtain a splitting of the lower Hubbard subband for arbitrary $\gamma$ and $V$. The resulting density of states per site can be expressed as

$$\rho(E)=N^{-1}\sum_k[A_k^-\delta(E-E_k^-)+A_k^+\delta(E-E_k^+)] \quad . \tag{30}$$

The coefficients $A_k^\pm$ are found from Eq. (27); their sum is equal to one.

We obtain from Eq. (29) a gap of $E_k^+-E_k^-$ for any finite $V$, thus missing the minimal $V=2|t|$ required for a gap in the exact[27] spectrum for $\gamma=0.5$. Of greater importance, however, is the demonstration of electronic excitations around $V$ for any $\gamma$, including $\gamma\neq 0.5$ where the spectrum is gapless. The bands $E_k^+$ and $E_k^-$ are shown in Fig. 2 for several densities $\gamma$. The bandwidths and CT transitions $E_k^+-E_k^-$ are almost independent of $\gamma$. The electron-hole symmetry $\mathcal{H}_{\rm red}$ ensures that $\gamma>0.5$ and $\gamma<0.5$ excitations coincide. This feature is unfortunately lost for finite $U$, when the analysis is far more difficult. The splitting of the lower Hubbard subband in Fig. 2 by an intersite Coulomb interaction $V$ thus entails no loss of symmetry in the regular chain. The resulting excitations around $V$ are weakly dependent on $\gamma$.

While more elaborate treatments of $\mathcal{H}_{\rm red}$ are possible, they probably have limited relevance unless the restriction $U\rightarrow\infty$ is relaxed. Furthermore, finding the oscillator strengths of the transitions around $V$ requires going beyond a density of states. For sufficiently large $U$, we still expect the two subbands in

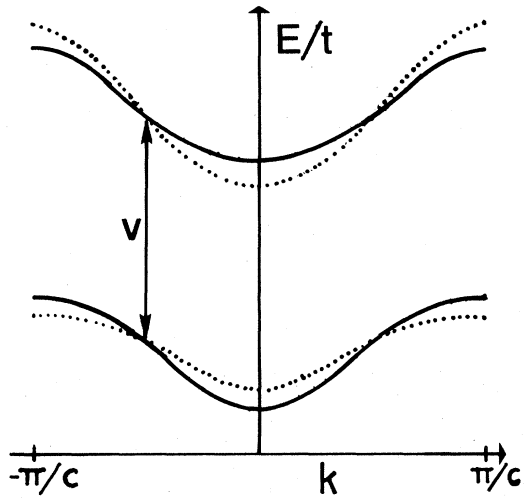


FIG. 2. Splitting of the lower Hubbard subband by a nearest-neighbor interaction $V=4|t|$, as given by Eq. (29) for $\gamma=0.50$ and $\gamma=0.70$. The CT transitions around $V$ are associated with the $A$ peak of $\gamma<1.0$ salts.

Fig. 2 to be separate, but with reduced splittings. The approximate treatment of $V$ in infinite systems will then guide exact results for CT transitions in finite systems with arbitrary $U$, $V$, and $|t|$.

## III. OPTICAL PROPERTIES

The Hubbard model (1), its extended form [Eq. (3)], its modified versions,[3] or the PPP model[24] all describe systems with precisely one valence state per site. We first note several general consequences of a restricted basis, which significantly alter the optical properties and have apparently not been discussed previously. These results hold for any spin-independent interactions $V_n$ between sites separated by $n$ lattice spacings and are not restricted to one-dimensional arrays. The Hamiltonian $\mathcal{H}$ then contains a transfer term, the $t$ term of Eq. (1), and various on-site and intersite interactions. For one valence state per site, the dipole moment operator[13] $\mu$ is

$$\mu=\sum_p\left(\frac{N+1}{2}n_p-pn_p\right) \tag{31}$$

for regular chain $N$ sites and lattice spacing $c$. The complete operator is $\mu ec$, where $e$ is the electronic charge. The number operator $n_p=0$, 1, or 2 describes the occupancy of the valence orbital. The corresponding dimensionless velocity operator $v$ is

$$v=\sum_{p\sigma}(a^{\dagger}_{p\sigma}a_{p+1\sigma}-a^{\dagger}_{p+1\sigma}a_{p\sigma}) \ . \tag{32}$$

The origin, which was taken at the midpoint of the chain in Eq. (31) no longer appears.

The oscillator strength[29] $f_{ks}$ of a transition from an exact eigenstate $|k\rangle$ to the exact eigenstate $|s\rangle$ is

$$f_{ks}=\omega_{sk}|\langle s|\mu|k\rangle|^2=|\langle s|v|k\rangle|^2\omega_{sk}^{-1} \ , \tag{33}$$

where $\hbar\omega_{sk}=E_s-E_k$ is the exact excitation energy. The sum rule[29] for transitions to all possible final states can be written as

$$F_k=\sum_s f_{ks}=2^{-1}\langle k|[[\mu,\mathcal{H}],\mu]|k\rangle \ . \tag{34}$$

Since, $\mu$ reduces to number operators for systems with one valence state per site $[\mu,n_pn_p']$ vanishes for arbitrary spin-independent interactions. We thus obtain

$$F_k=-\langle k|h_t|k\rangle \ , \tag{35}$$

where $h_t$ is the $t$ term of Eq. (1). The ground-state expectation value of $-h_t$ is positive and gives the total intensity of all CT processes at absolute zero.

Our result for $F_k$ should be contrasted with the usual Thomas-Reiche-Kuhn sum rule,[29] which goes as the number of electrons. The usual result is based on a complete set of states, rather than one valence state per site. The $t\rightarrow 0$ limit of Eq. (35) naturally suppressed all CT excitations, whereas conventionally including a complete set of molecular excitations would still yield the sum rule for individual molecules. The $U\rightarrow\infty$ limit of Eq. (35) also suppressed CT excitations for $\gamma=1$, since each site is then singly occupied and no charge motion can be induced by a field. The result has been discussed[30] for purely covalent VB diagrams, which provide an alternative statement of the $\gamma=1$, $U\rightarrow\infty$ limit. The exact sum rule (35) for restricted bases thus depends on $\gamma$, on $U/|t|$, and on the initial state $|k\rangle$. Care must consequently be taken in applying standard results to the optical properties of various extended or modified Hubbard models. We emphasize that the issue is internal consistency rather than the merits or deficiencies of Hubbard models.

We have previously obtained[11] exact eigenstates $|k\rangle$ by diagrammatic VB methods for cases with $N_e=4$ electrons on $N=4$, 5, 6, and 7 sites. All oscillator strengths $f_{ks}$ in Eq. (33) or sum rules $F_k$ in Eq. (35) can then be obtained[13] directly. Describing each transition at $\hbar\omega_{sk}$ by a Lorentzian $I_{ks}(z)$ normalized to $f_{ks}$ yields

$$I_{ks}(z)=f_{ks}\Gamma/\pi[(z-z_{sk})^2+\Gamma^2] \ , \tag{36}$$

where $z=\hbar\omega/\sqrt{2}|t|$ is a reduced energy and the half-width at half-height, $\Gamma$, is related to the excited-state lifetime. While the generalization to $\Gamma_{sk}$ is straightforward, such detailed parametrization is premature and a single adjustable $\Gamma$ is used in simulating CT spectra. The absolute absorption intensity $I_k(z)$ for

initial state $|k\rangle$ is found as usual[31]

$$I_k(z)=\frac{8\pi^3e^2a^2N_0}{chN}\sum_s I_{ks}(z)\ , \tag{37}$$

where $a$ is the lattice spacing, $c$ is the speed of light, $e$ is the electronic charge, $N_0$ is Avogadro's number, and $N$ is the size of the finite chain or ring. Such computations clearly require both energies and wave functions.

The extended Hubbard model, Eqs. (1) and (3), contains three parameters: $U$, $V$, and $|t|$. These are not restricted in direct numerical solutions. The nearest-neighbor interaction $V$ splits the lower Hubbard subband, as shown in Fig. 2, and is a candidate for the low-energy $A$ peaks in Table I. A finite $V$ also modifies the usual CT processes for the $B$ peak. Four electron cases illustrate all possible transitions for an infinite one-dimensional array. The simplier $N_e=2$ systems are inadequate in this respect. Representative CT processes are sketched in Fig. 3. The VB diagrams[11] have singlet-correlated, singly occupied sites denoted by lines, empty sites denoted by dots, and doubly occupied sites denoted by crosses. Diagrams with $S=1$ or 2 are shown by arrows connecting the singly occupied sites with parallel spins. The transition (a) in Fig. 3 changes the correlation energy by $V$. Changes of $U-2V$, $U-V$, $U$, $U+V$, $U+2V$, and $U-3V$ are also possible. The last is illustrated by (f) in Fig. 3 and requires a VB diagram with a doubly occupied site in the initial state. Such admixtures are small in the ground state for typical values, of $U$, $V$, and $|t|$. Thus both (e) and (f) are weak transitions, as are transitions around $U+2V$ that involve indirect coupling[32] of VB diagrams. The

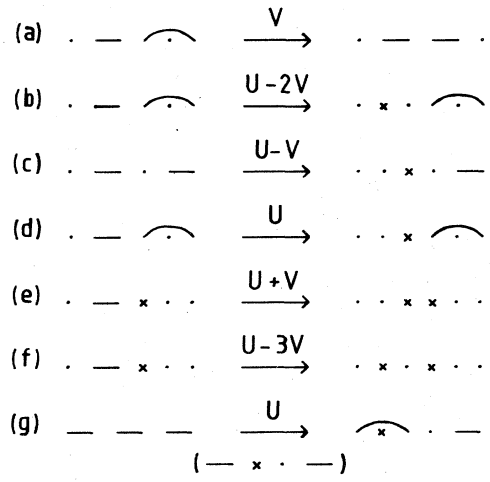


FIG. 3. Representative CT processes for singlet VB diagrams. Changes in the on-site ($U$) and nearest-neighbor ($V$) correlations are indicated. Unnormalized, symmetry-adapted linear combinations of such diagrams form the VB basis set.

most important CT processes for finite $V$ occur around $V$, $U-2V$, $U-V$, and $U$. It is readily seen that $N_e=2$ cases can only produce $V$ and $U-V$ transitions, while larger $N_e$ does not produce additional processes in one dimension. The many allowed CT processes for extended Hubbard models immediately suggest that the broad experimental bands are composites of many absorptions.

The $N_e=4$, $N=7$ ring is the smallest cyclic system with an absorption around $V$. The velocity operator $v$ in Eq. (32) commutes with the rotational quantum number $k$ and with the total spin $S$, but imposes an additional selection rule involving a reflection plane $\sigma$. VB diagrams in $\sigma=+$ and $-$ subspaces are illustrated in Fig. 4. It is readily seen that $\langle p|v|q\rangle\neq 0$ requires a change of $\sigma$ without changing $S$ or $k$. This additional symmetry requirement precludes transitions at $V$ in the $N_e=4$, $N=6$ ring. The $N_e=4$, $N=5$ ring has no excitations at $V$, since electron transfers like (a) in Fig. 3 conserve the number of $V$ interactions.

The ground state for any total $S$ for $N_e=4$, $N=7$ lies[32] in the $k=0$, $\sigma=+$ manifold whose dimension is 20 for $S=0$ and 18 for $S=1$. The $k=0$, $\sigma=-$ manifold has 8 VB kets for $S=0$ and 12 for $S=1$. For odd $N$ there is always at least one $V$ for $N_e=(N+1)/2$. The corresponding singlet VB ket appears only in the $\sigma=+$ manifold. All 8 singlet transitions in the $k=0$ subspace consequently involve energies of $V$ or more. The nature of the transitions can be identified from the VB functions in the $\sigma=-$ subspace. There are two transitions around $V$ involving VB diagrams without doubly occupied sites, one transition around $U-V$, two around $U$, and three weak transitions at higher energies. The position and oscillator strengths of the strong singlet CT transition are listed in Table II for several values of $z_0=U/\sqrt{2}|t|$ and $z_1=V/\sqrt{2}|t|$. These results are exact.

The triplet spectrum has the additional complication that a VB function with a single $V$ can occur in the $\sigma=-$ manifold of the $N_e=4$, $N=7$ ring. The lowest $S=1$ transition is an intraband process that

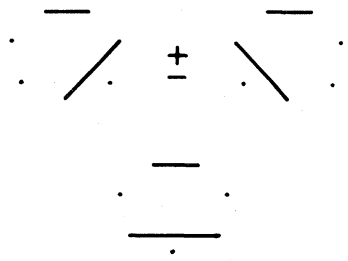


FIG. 4. Singlet VB diagrams for $N_e=4$ electrons on $N=7$ rings. The indicated linear combinations are even and odd with respect to a reflection plane and are in subspaces connected by dipole-allowed CT transitions.

TABLE II. CT transitions of $N_e=4$, $N=7$ rings from the lowest $S=0$ and $S=1$ states.

| Correlations $U/\sqrt{2}\|t\|$ | Correlations $V/\sqrt{2}\|t\|$ | Total spin $S$ | CT transitions[a] $\Delta E_A$ | $\Delta E_B$ | $\Delta E_C$ | Oscillator strengths[b] $F_A$ | $F_B$ | $F_C$ |
|---|---|---|---|---|---|---|---|---|
| 6 | 2 | 0 | 3.2926 | 6.6537 | 8.5182 | 0.0560 | 0.0171 | 0.0002 |
| | | | 5.0861 | | | | | |
| | | 1 | 3.5872 | 6.9046 | 9.2545 | 0.0670 | 0.0184 | 0.0002 |
| | | | 4.6460 | | | | | |
| | | | 5.0497 | | | | | |
| | | | 5.6640 | | | | | |
| 10 | 3 | 0 | 4.2440 | 9.2831 | 12.2710 | 0.0540 | 0.0234 | 0.0002 |
| | | | 5.884 | | | | | |
| | | 1 | 4.1556 | 9.4114 | 12.7343 | 0.0749 | 0.0369 | 0.0001 |
| | | | 5.3229 | | | | | |
| | | | 5.8683 | | | | | |
| | | | 6.4311 | | | | | |

[a]Units of $\sqrt{2}\|t\|$.

[b]Equations (33) and (35).

should not occur in an infinite chain. We have therefore classified[32] only 11 triplet transitions involving energies of $V$ or more. Exact results are given in Table II for several values of $z_0=U/\sqrt{2}\|t\|$ and $z_1=V/\sqrt{2}\|t\|$.

The absorptions in Table II can be grouped as $A$, $B$, and $C$ in order of increasing transition energies around $z_1$, $z_0-z_1$, and $z_0$, respectively. The total oscillator strengths $F_A$, $F_B$, and $F_C$ in Table II were obtained via Eq. (34) for transitions of any one kind. We note that $F_C$ is rather weak compared to $F_A$ and $F_B$. This higher-energy transition is probably masked by intramolecular excitations in TCNQ and TTF ion-radical salts. The oscillator strength $F_A$ exceeds $F_B$ by a factor of 2–3, indicating that the $V$ transition is the more intense. All other transitions at $2V$, $U+V$, etc., are less intense by at least two orders of magnitude.

There are no energy gaps for conduction in infinite partly filled regular stacks, nor for magnetic excitations in infinite half filled regular stacks. It is straightforward[13] in principle to consider the overall spectrum as involving a Boltzmann average over the $k$, $S$, $\sigma$ manifolds. These factors for small finite systems are, however, quite irrelevant as splittings of the order of $4\|t\|/N$ are inevitably found. The lowest $k=0$, $\sigma=+$ transitions in the $S=0$ and 1 manifolds in Table II are equally representative. They demonstrate that the complicated composite spectrum for thermally accessible excited states should, in fact, be largely temperature independent due to the close superposition of transitions from low-lying levels. Other low-lying states yield[13,32] similar results. The $A$ absorption becomes relatively more intense with increasing $S$, since the $B$ peak disappears in the ferromagnetic limit of all parallel spins. The lack of strong temperature dependences in the CT spectra of organic ion-radical salts, except possibly at phase transitions where the model parameters must change, provide strong qualitative support for our numerical results indicating similar CT spectra from various low-lying states. This is fortunate, as the exact analysis of larger systems rapidly becomes prohibitive.

Representative absorption spectra for $N_e=4$, $N=7$ rings are shown in Fig. 5, using (34) for the lowest $S=0$ and $S=1$ transitions. All broadening parameters $\Gamma$ were assigned the same value, as indicated. The line spectra in Fig. 5 show the exact individual energies and intensities of the CT bands. Such calculated results can be compared to the experimental data in Table I by identifying various processes, thereby associating an observed energy with dimensionless variable $E/\sqrt{2}\|t\|$ in Fig. 5. Such comparisons are pursued in the next section.

The $N_e=4$, $N=7$ ring has no transition around $U-2V$. The $N_e=4$, $N=6$ chain does have such a transition, as indicated by (b) in Fig. 3. The diagonal energies $V$ of chains are cyclized by considering sites 1 and 6 to be neighbors. Thus chains differ from rings in having no electron transfer, or $t$ term in Eq. (1), between the end sites. This spoils the rotational quantum number $k$. The VB basis functions are now classified[11,13] by their parity, $g$ and $u$ for even and odd, respectively. Dipole transitions[13] conserve $S$ and change parity. Finite chains, without the $k$ quantum number, have additional transitions of the intraband type involving covalent VB diagrams with identical $V$

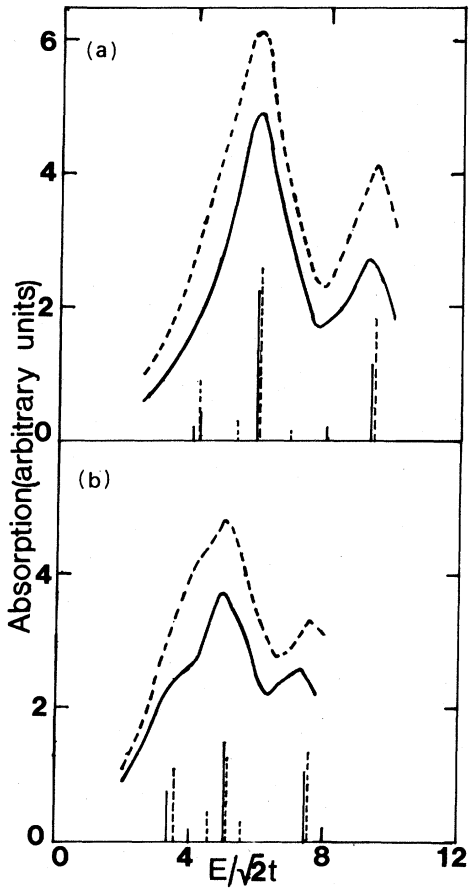


FIG. 5. Stick diagram and band spectra for the exact oscillator strengths, Eq. (33), of CT transitions for 4/7 rings with (a) $U/\sqrt{2}|t|=10$, $V/\sqrt{2}|t|=3$ and (b) $U/\sqrt{2}|t|=7$, $V/\sqrt{2}|t|=2$. Transitions from the lowest $S=0$ and $S=1$ subspaces are shown as solid and dashed lines, respectively. The resulting absorption curves, Eq. (36) have $\Gamma/\sqrt{2}|t|=1.0$ and a doubled intensity.

contributions. The analysis of Sec. II shows that these are artifacts of the small system, rather than features of infinite chains. The number of transitions without changing the minimal $V$ is ascertained from the VB diagrams, as is the number of transitions at $V$, $U-2V$, $U-V$, $U$, etc. The lowest $S=0$, $g$ subspace of the $N_e=4$, $N=6$ chain, for example, has four possible transitions at $V$, 3 at $U-2V$, and 6 at $U-V$, as shown in Table III for several values of $z_0=U/\sqrt{2}|t|$ and $z_1=V/\sqrt{2}|t|$. Even when both $V$ and $U-2V$ transitions are collected into $F_A$, the overall intensities $F_A$ and $F_B$ are quite comparable for the $(0,g)$ ground state. However, the lowest $S=1$, $g$ manifold and the lowest $S=0$, $u$ manifold yield strong transitions that favor $F_A$ over $F_B$, as summarized in Table III. The energy spreads of $A$ and $B$ transitions of $N_e=4$, $N=6$ chains are quite similar to those of $N_e=4$, $N=7$ rings, while the $F_A/F_B$ ratio is smaller for chains than rings.

The small sizes of chains and rings accessible to complete analysis restricts us to qualitative conclusions. We have mentioned various numerical procedures in excluding intraband transitions. As found previously,[11,33] partly filled rings with $N_e=4$ actually have triplet absolute ground states. The restrictions[34] imposed by the Pauli principle and the high rotational symmetry of regular rings also change the $U\rightarrow\infty$ limit. Most prominently, splittings on the order of $|t|$ persist for $\gamma<1$ rings. Partly filled chains are consequently better realizations[11] of the magnetic properties of the infinite system, while the inclusion of the wave vector $k$ suggests that rings are preferable for optical properties. The closely similar CT energies found for $\gamma=4/7$ rings and $\gamma=4/6$ chains supports the conclusion (29) that the $A$ transitions depend weakly on $\gamma$. The approximately similar intensity ratio $F_A/F_B\sim 2-3$ for chains and rings is a new result. These $N_e=4$ computations via diagram-

TABLE III. Total oscillator strengths of CT transitions of $N_e=4$, $N=6$ chains for the two lowest peaks.

| Correlations | | Ground states[a] | | Oscillator strength[b] /Transitions | |
|---|---|---|---|---|---|
| $U/\sqrt{2}\|t\|$ | $V/\sqrt{2}\|t\|$ | Spin | Parity | $F_A$ (No.)[c] | $F_B$ (No.)[c] |
| 6 | 2 | 0 | $g$ | 0.0448 (7) | 0.0411 (6) |
| | | 1 | $g$ | 0.2571 (11) | 0.1126 (6) |
| | | 1 | $u$ | 0.0307 (12) | 0.0278 (6) |
| | | 0 | $u$ | 0.3320 (11) | 0.0623 (6) |
| 10 | 3 | 0 | $g$ | 0.0351 (7) | 0.0537 (6) |
| | | 1 | $g$ | 0.2262 (11) | 0.1066 (6) |
| | | 1 | $u$ | 0.0163 (12) | 0.0277 (6) |
| | | 0 | $u$ | 0.3148 (11) | 0.1013 (6) |

[a]In increasing order of energy. [b]Equations (33) and (35). [c]Number of individual transitions.

matic VB methods[11] are the first direct solutions of partly filled extended Hubbard models in the intermediate regime $U > V > |t|$ and, as shown for $\gamma = 1$ CT transitions,[13] afford important improvements over dimer ($N_e = 2$) results.

## IV. DISCUSSION

The TTF halides in Table I provide the most convenient comparison of theory and experiment. First, their molecular excitations[14] start above 2 eV, thus leaving a larger window for CT processes and a more resolved $B$ peak. Second, the occurrence[35] of $(TTF^+)_2$ dimers in TTF-Cl fixes[14] the CT band at 1.5 eV as the normal dimer transition around $U - V$. This transition is virtually unshifted in the mixed-valence salts TTF-$X_\gamma$ and is the $B$ peak in Table I. The closely similar CT spectra of TTF-$Cl_{0.80}$, TTF-$Br_{0.79}$, and TTF-$I_{0.71}$ in Fig. 6 were obtained in Ref. 14. The indicated powder absorptions are consistent with single-crystal reflectivity data and with dimer transitions in solution. Intramolecular transitions, which dominate above 2 eV, are not shown. The similar optical properties of complex TCNQ salts in Table I encompass a variety of stacking patterns and of conductivities. The occurrence of several $|t|$'s in dimerized, trimerized, or tetramerized stacks has not been included. Differences in $|t|$ that are small compared to $V$ do not affect the optical spectra.

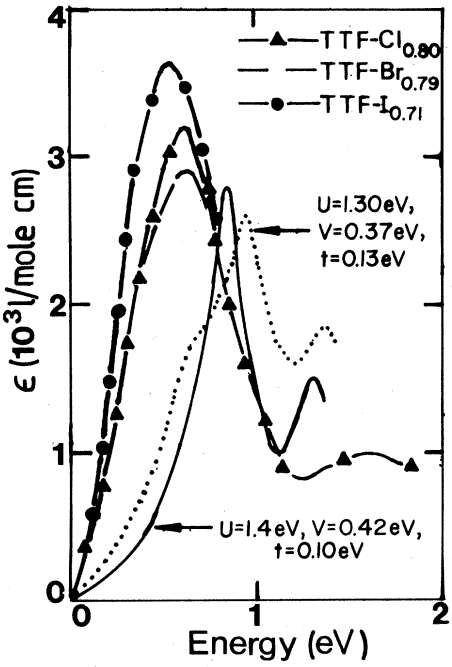


FIG. 6. Comparison of experimental absorption curves for mixed-valence TTF halides from Ref. 14 with extended Hubbard-model calculations for 4/7 rings. The theoretical curves are from Fig. 5 with the indicated parameter values. Their absolute intensity is discussed in the text.

The assignment of numerical values to $U$, $V$, and $|t|$ converts the reduced coordinates in Fig. 5 to actual energies. Furthermore, multiplying $\mu$ in Eq. (31) by $ea$, where $a$ is the lattice spacing, gives the absolute absorption intensity (37). The adjustable broadening parameter $\Gamma$ in Eq. (36) does not alter the area under the curve. Both theoretical curves in Fig. 6 are related to those in Fig. 5 for $\gamma = 4/7$ rings. The better fit is found for $|t| = 0.10$ eV, $U = 1.40$ eV, and $V = 0.42$ eV, with the $S = 0$ ground-state intensities scaled by a factor of 6 as discussed below. The observed $A$ peak around 0.6 eV is calculated at 0.79 eV while the observed $B$ peak around 1.5 eV is found at 1.33 eV. The observed separation between the two CT bands consistently exceeds the calculated values. The poorer theoretical fit in Fig. 6 is based on $|t| = 0.13$ eV, $U = 1.3$ eV, and $V = 0.38$ eV. The calculated $A$ peak is at still higher energy, while the calculated $B$ peak is at lower energy. We emphasize that the calculated curves are based on exact computations of extended Hubbard models and Lorentzian absorptions. We have deliberately omitted various vibronic, relaxation, and screening considerations that would undoubtedly improve the fit. Quite aside from introducing additional parameters, such processes require going beyond extended Hubbard models whose accurate solutions have been sought by VB methods. The restriction to rather small systems is, in this sense, the principal limitation.

The calculated absolute absorption coefficients lead in Eq. (37) to $A$ peaks of the order of 500–800 l/mol cm for the $S = 0$ or $S = 1$ ground state of either $N_e = 4$ or $N = 7$ rings or $N_e = 4$ or $N = 6$ chains. The next higher manifolds of chains have an order of magnitude larger $F_A$ and $F_B$, as shown in Table III. The sum rule [Eq. (35)] for a restricted basis thus depends, as expected, on the initial state. Partly filled molecular conductors have many thermally accessible states. While the CT transitions from low-lying manifolds are similar, their intensities vary by an order of magnitude. The calculated absorption coefficient of 500–5000 l/mol cm for the $A$ peak thus span the observed[14] value of 3000 l/mol cm. The relative intensities of the $A$ and $B$ peaks in Fig. 6 are slightly underestimated by our finite-ring results for $\gamma = 4/7 = 0.57$. The similar CT energies of 4/7 rings and 4/6 chains, as well as the weak $\gamma$ dependence of $E_k^+ - E_k^-$ in Eq. (29), lead us to rationalize discrepancies in terms of finite-size effects rather than the higher $\gamma$ of TTF halides. Approximate VB treatments of larger systems may allow testing this hypothesis.

The second point about the fit in Fig. 6 involves the magnitude of $|t|$ in TTF halides. The better fit has $|t| = 0.10$ eV and a bandwidth of $4|t| = 0.40$ eV; the poorer yields $|t| = 0.13$ eV and $4|t| = 0.52$ eV.

Still smaller $|t|$ would undoubtedly improve the fit to the optical data, but would nevertheless be inappropriate. The static susceptibilities[36] $\chi(T)$ of TTF salts are generally smaller than that of TTF-TCNQ, even when the latter is corrected for having two partly filled stacks. Our previous analysis[11] of $\chi(T)$ for $N_e=4$, $N=7$ chains led to a lower bound of $|t| \sim 0.15$ eV in TTF-TCNQ. While such an average for both stacks does not rule out a smaller $|t|$ for the TTF stack, the lower $\chi(T)$ of TTF salts actually suggests that $|t|$ should be larger. We are consequently reluctant to improve the optical fit by choosing $|t| < 0.10$ eV. It should be noted that other properties, like the sign of the thermopower,[37] are consistent with a smaller $|t|$ for $TTF^{+\gamma}$ stacks than for TCNQ stacks. Typical estimates[1-3,11,14] of $|t|$ are in the range 0.10–0.30 eV for either regular $TCNQ^{-\gamma}$ or $TTF^{+\gamma}$ stacks, and we cannot improve these from fitting optical spectra. Optical spectra involving vertical transitions may, or course, involve different values of $|t|$ than adiabatic contributions to the susceptibility. An explicit treatment of electron-phonon coupling would be needed to pursue this point.

The last comment about Fig. 6 involves the relative values of $U$ and $V$. Our choice of $U \simeq 3V$ agrees with theoretical values[26] based on including screening, but for somewhat smaller absolute values of $U=1.4$ eV, $V=0.42$ eV for the $|t|=0.10$ eV fit and $U=1.3$ eV, $V=0.37$ eV for the $|t|=0.13$ eV fit. Such values are consistent with previous analyses of optical properties. The $U-2V$ transitions then contribute to the broad and generally asymmetric $A$ peak in TTF and TCNQ salts. A representative CT process around $U-2V$, such as (b) of Fig. 3, involves three occupied sites next to an empty one. Such configurations increase for $\gamma > 0.5$, while configurations for $V$ transitions decrease, in qualitative support for the weak $\gamma$ dependence of $A$ transitions. Rather larger finite rings and chains will have to be analyzed, however, to test this hypothesis about the intensities of the overlapping $V$ and $U-2V$ transitions.

The next-higher-energy CT band, the $C$ peak around $U$ in Table II, has a substantially lower overall oscillator strength. The weak band may further be masked by intramolecular excitations. Yakushi, Kusaka, and Kuroda[38] have recently reported the low-temperature polarized reflectance spectrum of K-TCNQ, a $\gamma=1$ segregated stack that is *not* regular but has several types of TCNQ overlaps.[39] In addition to the principal CT peak around 1.0 eV, they find a weak low-temperature band around 1.4 eV. The strong ($B$) peak is around $U-V$ in the dimer model and is shifted[13] to somewhat lower energies in extended systems. The weak feature ($C$ peak) at 1.4 eV may then be associated with the weak transition at $U$. An estimate of $V \sim 0.4$ eV is quite consistent with our more detailed fit of the $A$ and $B$ peaks of TTF halides. A similar explanation for K-TCNQ has been proposed by Lyo,[40] who considers the $U-V$ band to be a local CT state below the upper Hubbard band at $U$. We consider instead the upper Hubbard subband to start around $U-V$ for half filled ($\gamma=1$) systems. The small admixture of $\cdots A^{-2}A^{-}A \cdots$ neighbors in the $\cdots A^{-}A^{-}A^{-} \cdots$ ground state then allows indirect CT transitions around $U$, as indicated in (g) of Fig. 3. Strong CT absorptions around $U-V$ and weak ones around $U$ are clearly shown by previous VB calculations[13] on half filled mixed or segregated regular stacks and by the present results for partly filled regular segregated stacks.

Band formation, as shown in Fig. 5, of CT transitions demonstrates that the broadening parameter $\Gamma$ in Eq. (36) cannot be routinely interpreted as an excited-state lifetime. Such a lifetime broadening reflects Drude or Drude-Lorentz fits of $I(\omega)$ in Eq. (37) for a single transition. For multiple transitions in infinite ion-radical stacks, however, there is a no *a priori* need for any lifetime broadening. The observed widths of CT transitions may reflect both band and lifetime contributions, as well as vibronic effects. The point is that $\Gamma$ values obtained from such fits may be quite unreliable for lifetimes.

We have already taken advantage of the exact wave functions in computing oscillator strengths for VB transitions. The ground state in any exact subspace of $S$, $k$, $\sigma$ can be expanded[11-13] in terms of VB diagrams. The situation $U > V > |t|$ is expected to favor configurations with no doubly occupied sites and as few adjacent electrons as possible. Such diagrams describe the exact ground state for $|t|=0$ and are closely related to Wigner lattice.[25] The main difference is that additional interactions $V_2$, $V_3$, . . . , are needed in Wigner lattices. In their absence, we naturally find similar weights[32] for diagrams with equal $V$ and different numbers of second or third neighbors. We denote VB diagrams with the minimum possible number of adjacent electrons as belonging to class I. All other covalent VB diagrams are in class II, while any VB diagram with one or more doubly occupied site is in class III. The decompositions of various ground states for fixed $U$, $V$, $|t|$, are listed in Table IV, which yields a quantitative assessment of CI in partly filled regular systems.

The rather low contribution of doubly occupied (class III) diagrams for the parameters in Table IV supports their exclusion, as done in Sec. II, in approximate treatments of extended Hubbard models. It is nevertheless just these class III diagrams that result in a non-Curie susceptibility. Somewhat larger values of $|t|$ are suggested by $\chi(T)$ data, as already mentioned, thereby increasing slightly the weight of doubly occupied sites. The point remains that small admixtures of doubly occupied sites suffice for the ground state, which is indeed close to the atomic limit for reasonable values of $U$, $V$, and $|t|$.

The effects of finite $V$ in partitioning between class

TABLE IV. Decomposition of lowest $S=0$ and $S=1$ VB states for $N_e=4$, $N=7$ rings.

| Correlations $U/\sqrt{2}\lvert t\rvert$ | Correlations $V/\sqrt{2}\lvert t\rvert$ | Total spin $S$ | Types of VB diagrams % class I | % class II | % class III |
|---|---|---|---|---|---|
| 6 | 0 | 0 | 43.13 | 54.69 | 2.18 |
| | | 1 | 39.09 | 55.56 | 5.35 |
| 10 | 0 | 0 | 44.66 | 54.43 | 0.91 |
| | | 1 | 42.17 | 55.58 | 2.25 |
| 6 | 2 | 0 | 70.44 | 26.23 | 3.33 |
| | | 1 | 64.88 | 27.87 | 7.25 |
| 7 | 2 | 0 | 71.57 | 26.10 | 2.33 |
| | | 1 | 67.04 | 27.73 | 5.23 |
| 9 | 3 | 0 | 80.73 | 17.71 | 1.56 |
| | | 1 | 77.62 | 18.88 | 3.50 |
| 10 | 3 | 0 | 81.17 | 17.64 | 1.19 |
| | | 1 | 78.58 | 17.97 | 2.70 |

I and class II diagrams are illustrated in Table IV by comparing $U/\sqrt{2}|t|=6$ results for $N_e=4$, $N=7$ rings. Only 43% of the ground state is in class I for $V=0$, as expected when class I is not favored. The class I contribution rises to 70% for $V/\sqrt{2}|t|=2$. The remaining class II contributions in Table IV for $V\sim 4|t|$ demonstrate sizable admixtures of configurations with additional interactions $V$. This is expected, since $V>4|t|$ is needed to stabilize the state with minimum numbers of adjacent electrons. Typical values of $V$ thus cannot be adequately described in the $|t|=0$ limit of only class I configurations.

For completeness, we mention several contrasting approaches to optical properties. Tanaka *et al.*[15] associate the $B$ peak of TCNQ salts with an intramolecular absorption. The higher intramolecular excitations of TTF halides does not fit such a picture, since their $B$ peak remains around 1.5 eV. A common theoretical approach to the CT spectra of partly filled regular stacks is certainly more attractive, as least as an initial hypothesis. Rice *et al.*[41] have recently assigned the $A$ peak in MEM(TCNQ)$_2$, a semiconducting complex salt below 335 K, to small site-energy differences and couplings to molecular vibrations within $(TCNQ)_2^-$ dimers. They do not comment on the $B$ peak. Any isolated $(TCNQ)_2^-$ dimer has an allowed transition at $2|t|$ between the bonding and antibonding MO, and differences of $2\delta$ in the site energies yield an $A$ peak at $2(t^2+\delta^2)^{1/2}$ for truly isolated dimers. It is not obvious, without independent evidence, that the dimer approximation with such widely varying transfer integrals ($t_{\text{intra}}=0.2$ eV, $t_{\text{inter}}=0$) is a reasonable starting point. The MEM(TCNQ)$_2$ absorptions are typical of the complex TCNQ salts in Table I, and we would assign them similarly, though transition energies and oscillator strengths could be expected to be modified slightly by differences in $t_{\text{intra}}$ and $t_{\text{inter}}$, site energies, etc. The final possibility, that phonon-assisted intraband transitions produce the $A$ peak, instead of nearest-neighbor interactions, would require very strong electron-phonon coupling. Duke[42] and Rice *et al.*[43] have obtained smaller electron-phonon coupling constants in various TCNQ insulators and semiconductors. Such strong coupling, furthermore, would dominate the dc transport in all organic conductors even at high temperature. Epstein *et al.*[44] have reported conductivity gaps in several disordered TCNQ salts and in a TCNQ alloy with variable filling. The small gaps ($\lesssim 1000$ K) at the Fermi energy are evidently sensitive to both the structure and the filling, in marked contrast to the low-energy CT peak around 5000 K in Table I. The peak resulting from $V$ persists in conductors with regular chains and involves a gap at $E_F$ only in the special case $\gamma=0.5$. The interpretation of small additional gaps suggested by transport studies is still open.

The magnetic properties of partly filled extended Hubbard models are qualitatively similar to those[11] with $V=0$. Exact results are lost for $V\neq 0$. Strong antiferromagnetic exchange interactions $J$ are again found. For $\gamma=1$ and $(U-V)\gg|t|$, we have $J=2t^2/(U-V)$, which simply involves an effective on-site correlation $U-V$. The situation is more complicated for $\gamma<1$, where there are several orbital manifolds[11] with splitting of order $|t|$ even in the $U\rightarrow\infty$ limit. Finite $V$ produces additional shifts. Any VB computation with $V=0$ can readily be done for $V\neq 0$. The resulting $\chi(T)$ for partly filled chains are qualitatively quite similar.

All Hubbard models are unrealistic in neglecting long-range Coulomb interactions. The low density of conduction electrons ($\gamma$ per molecule) and small bandwidth $4|t|$ of organic solids leads, at least for highly idealized models, to rather low plasma frequencies[45] that are only slightly higher than the $B$ peak. The direct observation of a plasmon, including

its dispersion, has been reported[46] in TTF-TCNQ and is in qualitative agreement with theory. Such experiments in other organic conductors would test the required density (or $\gamma$) dependence of plasmons. Both CT transitions discussed above are, by contrast, largely independent of $\gamma$ for $\gamma < 1$. Indeed, the insensitivity to filling led us to postulate the nearest-neighbor $V$ for the $A$ peak.

Low-lying plasmons, on the other hand, may imply frequency-dependent parameters $U$, $V$, and $|t|$ due to screening. We have neglected this possibility, whose detailed analysis certainly merits further attention, although the parameter values of Hubbard models can always be defined to include screening. The point is that a single value of $U$, $V$, and $|t|$ is taken for all CT transitions, as well as for thermal excitations contributing to transport and magnetic properties. Neglecting the likely frequency dependence for the parameters may then spoil comparison with experiment. Franck-Condon factors for optical transitions are another source for parameter differences between optical and thermal properties. As pointed out above, the $\chi(T)$ and CT transitions of organic conductors point to slightly different values of $|t|$. There are several candidates for improving the theory, but unfortunately none of them permit quantitative results.

In summary, nearest-neighbor interactions $V$ produce a new low-energy CT band around $V$ in partly filled extended Hubbard models and split the ususal CT band around $U$. The low-energy CT absorptions of TTF halides and of complex TCNQ salts have been associated with the $V$ and $U-2V$ transitions, while the usual CT band is assigned to $U-V$. Exact diagrammatic VB methods for four electrons on finite rings and chains yield both the position and intensities of CT transitions for $U \sim 3V$. These initial applications to partly filled infinite stacks are in fair agreement with experiment for typical values of $|t| \sim 0.10$–$0.15$ eV. The resulting CI picture of intermediate correlations, with $U \sim 3V$ and $V \sim 3|t|$, does not qualitatively alter the magnetism or conductivity of partly filled ($0.5 \leq \gamma \leq 1.0$) Hubbard models.

## ACKNOWLEDGMENTS

We thank Dr. S. R. Bondeson and Professor D. J. Klein for numerous discussions about this work. The financial support of the Grant No. NSF DMR-7727418 A01 is gratefully acknowledged.

[1] *Chemistry and Physics of One-Dimensional Metals,* edited by H. J. Keller (Plenum, New York, 1977); *Physics and Chemistry of Low-Dimensional Solids,* edited by L. Alcazer (Plenum, New York, 1980, in press).

[2] J. S. Miller and A. J. Epstein, Ann. N. Y. Acad. Sci. 313 (1978); *Lecture Notes in Physics 96, Quasi One-Dimensional Conductors II,* edited by S. Barisic *et al.* (Springer, New York, 1979).

[3] Z. G. Soos and D. J. Klein, in *Molecular Association,* edited by R. Foster (Academic, New York, 1975), Vol. 1, pp. 1–109; Z. G. Soos, Annu. Rev. Phys. Chem. 25, 121 (1974).

[4] F. H. Herbstein, in *Perspectives in Structural Chemistry,* edited by J. D. Dunitz and J. A. Ibers (Wiley, New York, 1971), Vol. IV, pp. 165–395.

[5] P. L. Nordio, Z. G. Soos, and H. M. McConnell, Annu. Rev. Phys. Chem. 17, 237 (1966).

[6] W. J. Siemons, P. E. Bierstedt, and R. G. Kepler, J. Chem. Phys. 39, 3523 (1963).

[7] Y. Iida, Bull. Chem. Soc. Jpn. 42, 637 (1969).

[8] J. Hubbard, Proc. R. Soc. London Ser. A 276, 238 (1963); 277, 237 (1964); 281, 401 (1964); 285, 542 (1965).

[9] J. B. Torrance, Acc. Chem. Res. 12, 79 (1979).

[10] Z. G. Soos, and S. Mazumdar, Phys. Rev. B 18, 1991 (1979); Z. G. Soos, S. R. Bondeson, and S. Mazumdar, Chem. Phys. Lett. 65, 331 (1979).

[11] S. Mazumdar and Z. G. Soos, Synth. Met. 1, 77 (1979); S. R. Bondeson and Z. G. Soos, J. Chem. Phys. 71, 3807 (1979).

[12] Z. G. Soos and S. R. Bondeson, Solid State Commun. 35, 11 (1980) S. R. Bondeson and Z. G. Soos, Phys. Rev. B 22, 1793 (1980).

[13] S. R. Bondeson and Z. G. Soos, Chem. Phys. 44, 403 (1979).

[14] J. B. Torrance, B. A. Scott, B. Welber, F. B. Kaufam, and P. E. Seiden, Phys. Rev. B 19, 730 (1979).

[15] J. Tanaka, M. Tanaka, T. Kawai, T. Takabe, and O. Maki, Bull. Chem. Soc. Jpn. 49, 2358 (1976).

[16] J. B. Torrance, B. A. Scott, and F. B. Kaufman, Solid State Commun. 17, 1369 (1975).

[17] R. S. Mulliken, J. Am. Chem. Soc. 74, 811 (1952); J. Phys. Chem. 56, 801 (1952); R. S. Mulliken and W. B. Person, *Molecular Complexes: A Lecture and Reprint Volume* (Wiley, New York, 1969).

[18] N. F. Mott, Proc. R. Soc. London 62, 416 (1949).

[19] D. J. Klein and Z. G. Soos, Mol. Phys. 20, 1013 (1971).

[20] G. Beni, T. Holstein, and P. Pincus, Phys. Rev. B 8, 312 (1973); D. J. Klein, *ibid.* 8, 3452 (1973).

[21] E. H. Lieb and F. Y. Wu, Phys. Rev. Lett. 20, 1445 (1968).

[22] A. A. Ovchinnikov, Zh. Eksp. Teor. Fiz. 57, 2137 (1969) [Sov. Phys. JETP 30, 1100 (1970].

[23] G. V. Uimin and S. V. Fomichev, Sov. Phys. JETP 36, 1001 (1973); C. F. Coll, III, Phys. Rev. B 9, 2150 (1974).

[24] R. Pariser and R. G. Parr, J. Chem. Phys. 21, 446, 767 (1953); A. J. Pople, Trans. Faraday Soc. 42, 1375 (1953).

[25] G. Beni and P. Pincus, Phys. Rev. B 9, 2963 (1974); J. F. Kwak and G. Beni, *ibid.* 13, 674 (1976).

[26] J. Hubbard, Phys. Rev. B 17, 494 (1978).

[27] J. des Cloizeaux and M. Gaudin, J. Math. Phys. 7, 1384 (1966); J. des Cloizeaux, *ibid.* 7, 2136 (1966).

[28]D. N. Zubarev, Sov. Phys. Usp. 3, 320 (1960).
[29]See, for example, E. Merzbacher, *Quantum Mechanics* (Wiley, New York, 1961), pp. 445–459.
[30]C. Sandorfy, *Electronic Spectra and Quantum Chemistry* (Prentice-Hall, Englewood Cliffs, 1964), Chap. 9.
[31]See, for example, P. W. Atkins, *Physical Chemistry* (Freeman, San Fransico, 1978), pp. 585–87.
[32]S. Mazumdar, Ph.D. thesis (Princeton University, 1980) (unpublished).
[33]Z. G. Soos, S. Mazumdar, and T. T. P. Cheung, in *Molecular Metals,* edited by W. E. Hatfield (Plenum, New York, 1979), pp. 141–48.
[34]D. J. Klein (private communication).
[35]B. A. Scott, S. J. LaPlaca, J. B. Torrance, B. D. Silverman, and B. Welber, J. Am. Chem. Soc. 99, 6631 (1977).
[36]F. Wudl, D. E. Schafer, W. M. Walsh, Jr., L. W. Rupp, F. J. DiSalvo, J. V. Waszczak, M. L. Kaplan, and G. A. Thomas, J. Chem. Phys. 66, 377 (1977).
[37]P. M. Chaikin, J. F. Kwak, T. E. Jones, A. F. Garito, and A. J. Heeger, Phys. Rev. Lett. 31, 601 (1973).
[38]K. Yakushi, T. Kusaka, and H. Kuroda, Chem. Phys. Lett. 68, 139 (1979).
[39]A. Hoekstra, T. Spoelder, and A. Vos, Acta Crystallogr. Sect. B 28, 14 (1972), and references therein.
[40]S. K. Lyo, Phys. Rev. B 18, 1854 (1978).
[41]M. J. Rice, V. M. Yartsev, and C. S. Jacobsen, Phys. Rev. B 21, 3437 (1980).
[42]C. B. Duke, Ann. N. Y. Acad. Sci. 313, 166 (1978).
[43]M. J. Rice, N. O. Lipari, and S. Strassler, Phys. Rev. Lett. 39, 1359, (1977).
[44]A. J. Epstein, E. M. Conwell, and J. S. Miller, Ann. N.Y. Acad. Sci. 313, 183 (1978).
[45]P. F. Williams and A. N. Bloch, Phys. Rev. B 10, 1097 (1974).
[46]J. J. Ritsko, D. J. Sandman, A. J. Epstein, P. C. Gibbons, S. E. Schnatterly, and J. Fields, Phys. Rev. Lett. 34, 1330 (1975).